

# Energy Spectra in Quantum Fluid Turbulence

Kyo Yoshida and Toshihico Arimitsu

*Department of Physics, Graduate School of Pure and Applied Sciences,  
University of Tsukuba, 1-1-1 Tennoudai, Tsukuba, Ibaraki 305-8571, Japan*

Reprint of *J. Low Temp. Phys.* **145**, 219—230 (2006).

<http://springerlink.metapress.com/content/3687g562821355h3>

The original publication is available at [www.springerlink.com](http://www.springerlink.com).

*The Gross-Pitaevskii equation describes the dynamics of quantum fluids such as superfluids and Bose-Einstein condensates. Numerical simulations of turbulence obeying the Gross-Pitaevskii equation with forcing and dissipation are performed. The interaction energy spectrum obeys the scaling law  $E^{\text{int}}(k) \propto k^{-3/2}$ , which is consistent with the weak turbulence analysis. However, in contradiction to the assumptions in the weak turbulence analysis, it is found that the density fluctuation is not small and that the frequency spectrum does not have narrow peaks. Another possibility to explain the scaling law is discussed.*

*PACS numbers: 47.27.Gs, 47.37.+q, 67.40.Vs*

## 1. INTRODUCTION

Dynamics of low-temperature superfluids and Bose-Einstein condensates are described by the Gross-Pitaevskii (GP) equation<sup>1,2</sup> (also called the nonlinear Schrödinger equation),

$$i\hbar \frac{\partial}{\partial t} \psi = - \left( \frac{\hbar^2}{2m} \nabla^2 + \mu \right) \psi + g|\psi|^2 \psi, \quad (1)$$

under a certain approximation. Here,  $\psi := \langle \hat{\psi} \rangle$  is the order parameter, the average of a boson field  $\hat{\psi}$ ,  $m$  is the mass of the boson,  $\mu$  is the chemical potential, and  $g$  is the coupling constant. The chemical potential  $\mu$  may be related to  $n := |\psi|^2$  by  $\mu = g\bar{n}$  where the bar  $\bar{\phantom{x}}$  denotes the spatial average. Equation (1) may be interpreted as the equations of motion for fluid with density  $\rho$  and velocity  $\mathbf{v}$  by the use of Madelung's transformation  $\psi = \sqrt{\rho/m} e^{i\varphi}$  with  $\mathbf{v} := (\hbar/m)\nabla\varphi$ . Here, we call the fluid *quantum fluid*.

## K. Yoshida and T. Arimitsu

The quantum fluid is in some aspects different from the conventional classical fluid which obeys the Navier-Stokes equations. For example, the quantum fluid has no vorticity  $\omega := \nabla \times \mathbf{v}$  wherever  $\mathbf{v}$  is defined, *i.e.*  $\rho \neq 0$ , and the vorticity must be concentrated in lines where  $\rho = 0$ . The circulations around such lines are quantized due to the uniqueness of the phase  $\varphi$  up to modulus of  $2\pi$ . On the other hand, circulation can take an arbitrary value in classical fluid.

In spite of such differences between quantum and classical fluids, it has been known from recent studies that there are some similarities between quantum and classical fluid turbulence. It is well accepted from experiments<sup>3</sup> and direct numerical simulations<sup>4</sup> that the energy spectrum  $E(k)$  in the homogeneous and isotropic classical fluid turbulence at high Reynolds number obeys Kolmogorov's  $k^{-5/3}$  law within some accuracy. Recent experiments of turbulence in superfluid phase of liquid  $^4\text{He}$  are showing some evidence that the energy spectrum obeys the same Kolmogorov's  $k^{-5/3}$  law<sup>5,6</sup>. The Kolmogorov energy spectrum is also observed in numerical simulations of the GP equation<sup>7-9</sup>. These experimental and numerical results suggest that there is an energy cascade process not only in classical fluid turbulence but also in quantum fluid turbulence.

Details of the cascade process and the turbulence statistics should depend on the governing equation, especially on the form of its nonlinear terms. In order to investigate the cascade process and the statistics in quantum fluid turbulence in detail, we performed numerical simulations of homogeneous and quasi-isotropic turbulence obeying the GP equation with forcing and dissipation. In this paper, we will report some results obtained from the simulations.

## 2. BASIC EQUATION AND STATISTICAL QUANTITIES

For the sake of convenience in the numerical simulation, we introduce a normalization,  $\tilde{\mathbf{x}} := \mathbf{x}/\ell$ ,  $\tilde{t} := (g\bar{n}/\hbar)t$ ,  $\tilde{\psi} := (1/\sqrt{\bar{n}})\psi$ , which yields a normalized GP equation,

$$i\frac{\partial\tilde{\psi}}{\partial\tilde{t}} = -\tilde{\xi}^2\tilde{\nabla}^2\tilde{\psi} - \tilde{\psi} + |\tilde{\psi}|^2\tilde{\psi}, \quad (2)$$

with  $\tilde{\xi} := \xi/\ell$  where  $\xi := \hbar/\sqrt{2mg\bar{n}}$  is the healing length, and  $\ell$  is an arbitrary unit length scale. In the following of this paper, we will deal with the normalized variables and the normalized equation (2), and the tilde  $\tilde{\phantom{x}}$  will be omitted.

The density field and the velocity field of the quantum fluid are given by  $\rho := |\psi|^2$  and  $\mathbf{v} := 2\xi^2\nabla\varphi$ , respectively, in the present normalization. The

## Energy Spectra in Quantum Fluid Turbulence

density fluctuation is given by  $\delta\rho := \rho - \bar{\rho}$ , where  $\bar{\rho} = 1$ . Note that when  $\psi$  is almost uniform and its relative fluctuation from the mean is small, *i.e.*,

$$\psi = \psi_0 + \delta\psi, \quad |\delta\psi| \ll |\psi_0| = 1, \quad (3)$$

Eq. (2) admits the wave solution  $\delta\psi \propto e^{i(\mathbf{k}\cdot\mathbf{x} + \Omega_k t)}$  with the dispersion relation,

$$\Omega_k = \pm \xi k \sqrt{2 + \xi^2 k^2}, \quad (4)$$

where  $k := |\mathbf{k}|$ .

In the numerical simulation, we apply periodic boundary conditions with periods  $2\pi$  in each of three directions in the Cartesian coordinates for simplicity. Under these boundary conditions, it is convenient to introduce the Fourier space representation of (2),

$$\begin{aligned} \frac{\partial}{\partial t} \psi_{\mathbf{k}} &= -i\xi^2 k^2 \psi_{\mathbf{k}} + i\psi_{\mathbf{k}} - i \sum_{\mathbf{k}+\mathbf{p}-\mathbf{q}-\mathbf{r}=\mathbf{0}} \psi_{\mathbf{p}}^* \psi_{\mathbf{q}} \psi_{\mathbf{r}} \\ &+ D_{\mathbf{k}} + F_{\mathbf{k}}, \end{aligned} \quad (5)$$

where the Fourier transform of an arbitrary function  $f(\mathbf{x})$  and its inverse are given by

$$f_{\mathbf{k}} := \frac{1}{(2\pi)^3} \int d\mathbf{x} f(\mathbf{x}) e^{-i\mathbf{k}\cdot\mathbf{x}}, \quad f(\mathbf{x}) = \sum_{\mathbf{k}} f_{\mathbf{k}} e^{i\mathbf{k}\cdot\mathbf{x}},$$

with  $\mathbf{k} = (k_1, k_2, k_3)$ ,  $k_1, k_2, k_3 = 0, \pm 1, \pm 2, \dots$ . In (5), a dissipation term  $D_{\mathbf{k}}$  and a forcing term  $F_{\mathbf{k}}$  are added to the original equation (2).

The dissipation term  $D_{\mathbf{k}}$  should originate in the interaction between  $\psi$  and the fluctuation,  $\delta\hat{\psi} := \hat{\psi} - \psi$ , which is neglected in (2). We may expect that the dissipation term mainly acts in a high wavenumber range and that some statistics of  $\psi$  in the inertial subrange are insensitive to the details of the dissipation mechanism. In the present study, we will not discuss the dissipation mechanism further and use a Laplacian type model,

$$D_{\mathbf{k}} = -\nu k^2 \psi_{\mathbf{k}}, \quad (6)$$

for simplicity. In the present study, we will focus our interest on the wavenumbers smaller than  $\xi^{-1}$ . Note that the typical time scale of the dissipation is given by  $\tau_d(k) = \nu^{-1} k^{-2}$  and that the waves with wavenumber  $k$  may be efficiently dissipated when  $\tau_d(k) < \Omega_k^{-1}$ . Hence,  $\nu \sim \xi^2$  implies that the modes with  $k > \xi^{-1}$  are efficiently dissipated and that the modes with  $k < \xi^{-1}$  are less influenced by the artificial dissipation. We put  $\nu = \xi^2$  in the present simulations.

## K. Yoshida and T. Arimitsu

Due to the dissipation term  $D_{\mathbf{k}}$ , the mean density  $\bar{\rho}$  is not conserved any more and decays with time. In order to achieve a statistically quasi-stationary state, it is necessary to pump the density. The pumping is introduced by amplifying low wavenumber modes, *i.e.*,  $F_{\mathbf{k}}$  is given by

$$F_{\mathbf{k}} = \begin{cases} \alpha\psi_{\mathbf{k}} & (k < k_f) \\ 0 & (k \geq k_f) \end{cases}, \quad (7)$$

where  $\alpha$  is determined at every time step so as to keep  $\bar{\rho}$  almost unity.

It may be worthwhile to mention here that Kobayashi and Tsubota<sup>8</sup> (hereafter KT) introduced a different type of dissipation and forcing in their numerical simulation of GP turbulence. The equation in their simulation is given by

$$\begin{aligned} \hbar(i - \gamma^*) \frac{\partial}{\partial t} \psi &= - \left( \frac{\hbar^2}{2m} \nabla^2 + \mu(t) \right) \psi + g|\psi|^2 \psi \\ &+ W(\mathbf{x}, t) \psi, \end{aligned} \quad (8)$$

where  $\gamma$  is a function whose Fourier transform  $\gamma_{\mathbf{k}}$  is given by  $\gamma_{\mathbf{k}} = \gamma_0(k > 2\pi/\xi)$ ,  $\gamma_{\mathbf{k}} = 0(k \leq 2\pi/\xi)$ , and  $*$  denotes convolution. The time-dependent chemical potential  $\mu(t)$  is introduced to conserve  $\bar{\rho}$ . The system is forced by the random potential  $W(\mathbf{x}, t)$  with a large correlation length  $L_0 \gg \xi$ . The term with  $\gamma$  induces a corresponding dissipation term  $D_{\mathbf{k}}$  which is not a linear function of  $\psi_{\mathbf{k}}$  but a nonlinear function of  $\psi_{\mathbf{k}'}$  where  $\mathbf{k}'$  may be an arbitrary wavevector.

Let us introduce the statistical quantities which will be investigated in the present study. The kinetic and interaction energy density per unit mass,  $E^{\text{kin}}$  and  $E^{\text{int}}$ , respectively, are given by

$$E^{\text{kin}} := \frac{1}{V} \int d\mathbf{x} \xi^2 |\nabla \psi|^2 = \sum_{\mathbf{k}} \xi^2 k^2 \psi_{\mathbf{k}}^2, \quad (9)$$

$$E^{\text{int}} := \frac{1}{2V} \int d\mathbf{x} (\delta\rho)^2 = \sum_{\mathbf{k}} |(\delta\rho)_{\mathbf{k}}|^2, \quad (10)$$

where  $V$  is the volume of the domain. The kinetic energy  $E^{\text{kin}}$  can be divided into three parts,

$$E^{\text{kin}} = E^{\text{wi}} + E^{\text{wc}} + E^{\text{q}}, \quad (11)$$

$$E^{\text{wi}} := \frac{1}{2V} \int d\mathbf{x} |\mathbf{w}^{\text{i}}|^2, \quad E^{\text{wc}} := \frac{1}{2V} \int d\mathbf{x} |\mathbf{w}^{\text{c}}|^2, \quad E^{\text{q}} := \frac{1}{V} \int d\mathbf{x} \xi^2 |\nabla \sqrt{\rho}|^2, \quad (12)$$

where

$$\mathbf{w} := \frac{1}{\sqrt{2}\xi} \sqrt{\rho} \mathbf{v}, \quad (13)$$

## Energy Spectra in Quantum Fluid Turbulence

Table 1. Parameters in the numerical simulations.

	$N$	$k_{\max}$	$\xi$	$\nu(\times 10^{-3})$	$k_f$	$\Delta t$	$\bar{\rho}$
RUN128	128	60	0.05	2.5	2.5	0.01	0.998
RUN256	256	120	0.025	0.625	2.5	0.01	0.999
RUN512	512	241	0.0125	0.15625	2.5	0.01	0.998

and  $\mathbf{w}^i$  and  $\mathbf{w}^c$  are, respectively, incompressible and compressible parts of  $\mathbf{w}$ , *i.e.*,  $\mathbf{w} = \mathbf{w}^i + \mathbf{w}^c$ ,  $\nabla \cdot \mathbf{w}^i = 0$ , and  $\nabla \times \mathbf{w}^c = 0$ . In contrast to the more conventional decomposition  $\sqrt{\rho}\mathbf{v} = \sqrt{\rho}\mathbf{v}^i + \sqrt{\rho}\mathbf{v}^c$ , the present decomposition  $\mathbf{w} = \mathbf{w}^i + \mathbf{w}^c$ , which was introduced in Ref. 10, has the advantage of not involving a mixed compressible-incompressible energy.

Energy spectra associated with the energies  $E^{\text{kin}}$ ,  $E^{\text{int}}$ ,  $E^{\text{wi}}$ ,  $E^{\text{wc}}$ , and  $E^{\text{q}}$  are defined by

$$E^{\text{kin}}(k) := \sum_{k'=k} \xi^2 k'^2 |\psi_{\mathbf{k}'}|^2, \quad E^{\text{int}}(k) := \sum_{k'=k} |(\delta\rho)_{\mathbf{k}'}|^2, \quad (14)$$

$$E^{\text{wi}}(k) := \frac{1}{2} \sum_{k'=k} |\mathbf{w}_{\mathbf{k}'}^i|^2, \quad E^{\text{wc}}(k) := \frac{1}{2} \sum_{k'=k} |\mathbf{w}_{\mathbf{k}'}^c|^2, \quad (15)$$

$$E^{\text{q}}(k) := \sum_{k'=k} \xi^2 k'^2 |(\sqrt{\rho})_{\mathbf{k}'}|^2, \quad (16)$$

where  $\sum_{k'=k}$  denotes the summation with respect to  $\mathbf{k}'$  over the shell  $k - 1/2 < |\mathbf{k}'| \leq k + 1/2$ .

### 3. NUMERICAL SIMULATION

#### 3.1. Set up

We performed the numerical simulations of (5) by using an alias-free spectral method. A 4th-order Runge-Kutta method is used for the time marching. We performed three simulations which will be denoted by RUN128, RUN256, and RUN512. Parameters in the numerical simulations are listed in Table 1, where  $N$  is the number of grid points along each of the Cartesian coordinates in real space,  $k_{\max}$  is the maximum wavenumber, and  $\Delta t$  is the time step. The healing length  $\xi$  is the smallest length scale of interest in the present study. We employed a criterion  $k_{\max}\xi \sim 3$  in order that the length scale  $\xi$  is resolved in the simulations. The initial fields of RUN128 and RUN256 were given by  $|\psi_{\mathbf{k}}| = Ck^2 \exp(k^2/k_p^2)$  with random phases, where  $k_p = 2$  and  $C$  is determined from the constraint  $\bar{\rho} = 1$ . The initial field of

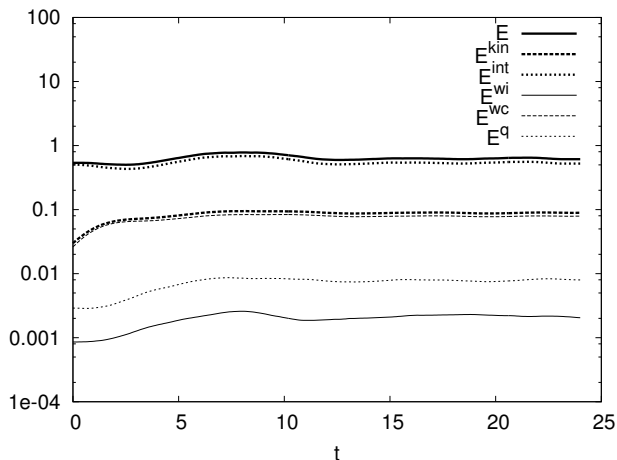


Fig. 1. The time evolution of the energies  $E$ ,  $E^{\text{int}}$ ,  $E^{\text{kin}}$ ,  $E^{\text{wi}}$ ,  $E^{\text{wc}}$ , and  $E^{\text{q}}$  in RUN512.

RUN512 is a statistically quasi-stationary state of RUN256 ( $t=20$ ). Most of the results presented in this paper are those from RUN512.

### 3.2. Energies and Energy Spectra

The time evolution of the energies  $E := E^{\text{int}} + E^{\text{kin}}$ ,  $E^{\text{int}}$ ,  $E^{\text{kin}}$ ,  $E^{\text{wi}}$ ,  $E^{\text{wc}}$ , and  $E^{\text{q}}$  in RUN512 are given in Fig. 1. Each energy is nearly constant in time after an initial transient period. One can see from the figure that  $E^{\text{int}}$  occupies 85% of the total energy  $E$ . The remaining 15% is  $E^{\text{kin}}$  which consists of  $E^{\text{wi}}$ ,  $E^{\text{wc}}$ , and  $E^{\text{q}}$ . The energy  $E^{\text{wi}}$  is about 40 times smaller than  $E^{\text{wc}}$ . Energy spectra  $E^{\text{kin}}(k)$ ,  $E^{\text{int}}(k)$ ,  $E^{\text{wi}}(k)$ ,  $E^{\text{wc}}(k)$ , and  $E^{\text{q}}(k)$  in RUN512 at  $t = 24$  are shown in Fig. 2. The scaling of  $E^{\text{wi}}(k)$  is not clearly observed. These results are in strong contrast to those of the numerical simulation in KT, in which  $E^{\text{wi}}$  is about 4 times larger than  $E^{\text{wc}}$  and the Kolmogorov spectrum  $E^{\text{wi}}(k) \propto k^{-5/3}$  is observed.

Possible origins of the discrepancy between the results in the present study and in KT are the difference in the forcing and the dissipation applied to each simulation. We may suppose that the forcing is more responsible for the difference in the energy ratio  $E^{\text{wi}}/E^{\text{wc}}$ , since the forcing mainly acts in the low wavenumber range, *i.e.*, the energy containing range, whereas the dissipation mainly acts in the high wavenumber range. The present result  $E^{\text{wi}} \ll E^{\text{wc}}$ ,  $E^{\text{int}}$  suggests that the forcing  $F_{\mathbf{k}}$  of the form (7) scarcely injects energy into  $E^{\text{wi}}$ . Note that  $E^{\text{wi}}(k)$  is smaller than  $E^{\text{wc}}(k)$  not only in the

## Energy Spectra in Quantum Fluid Turbulence

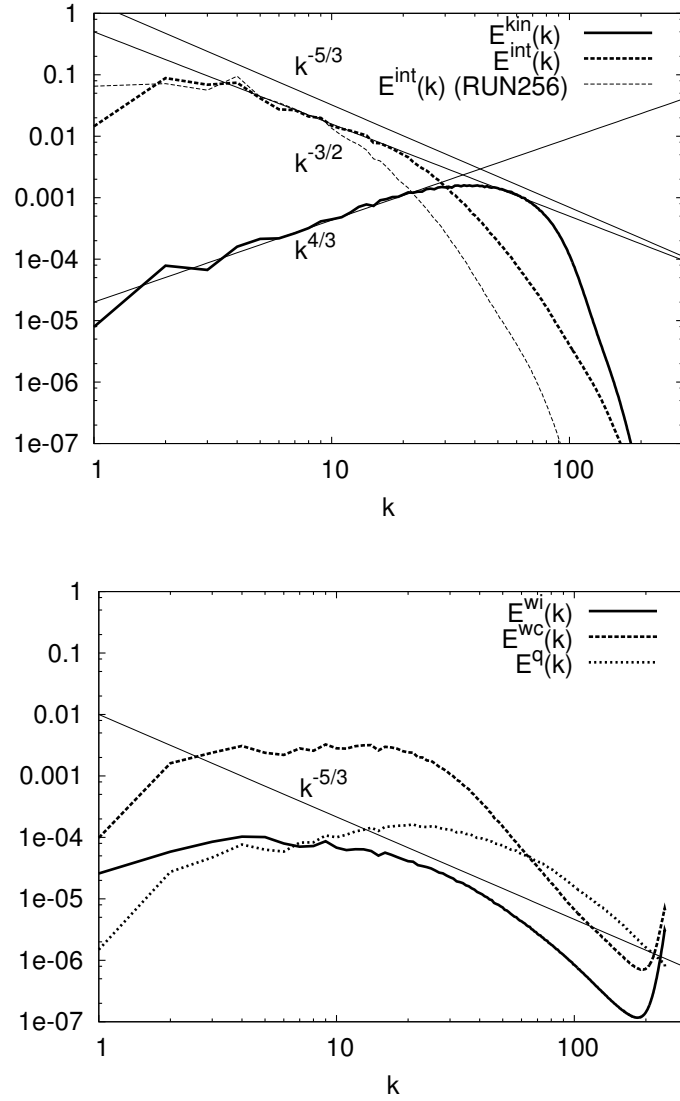


Fig. 2. Energy Spectra in RUN512 at  $t = 24$ .  $E^{\text{kin}}(k)$  and  $E^{\text{int}}(k)$  in the top figure, and  $E^{\text{wi}}(k)$ ,  $E^{\text{wc}}(k)$ , and  $E^{\text{q}}(k)$  in the bottom figure.  $E^{\text{int}}(k)$  in RUN256 at  $t = 20$  is also given in the top figure.

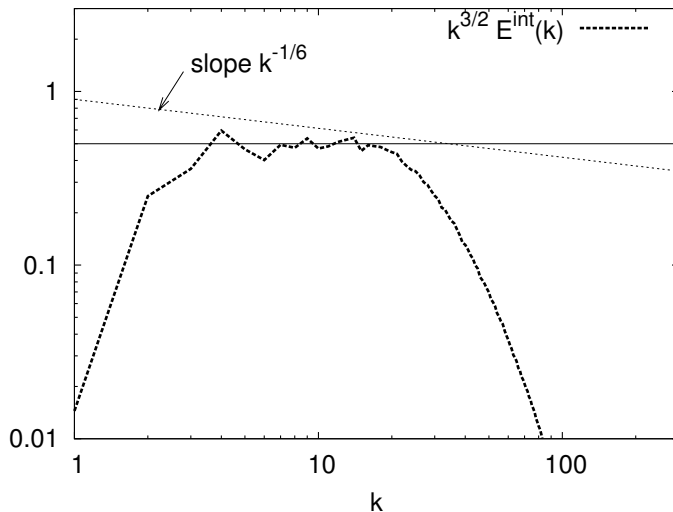


Fig. 3. Compensated Energy Spectrum  $k^{3/2}E^{\text{int}}(k)$  in RUN512 at  $t = 24$ . An arbitrary constant line and the slope  $k^{-1/6}$  are given for reference.

low wavenumbers range but also in the high wavenumbers where the forcing is not directly applied. This suggests that the coupling between  $\mathbf{w}^i$  and  $\mathbf{w}^c$  is weak and that the energy is not efficiently transferred from  $E^{\text{wc}}$  to  $E^{\text{wi}}$ . Hence, we may conclude that the scaling of  $E^{\text{wi}}(k)$  is not observed in the present simulation because the turbulence is moderately developed with respect to  $\mathbf{w}^i$  due to the scarce injection and transfer of energy to  $\mathbf{w}^i$ .

Comparison between KT and the present study suggests that energy spectra in the inertial subrange are not universal, *i.e.*, they depend on the forcing applied outside the inertial subrange. If this is the case, it is of interest to investigate how the inertial subrange statistics is affected by the forcing.

Let us analyze the turbulence statistics for the present case further. As shown in Fig. 2, it is found that  $E^{\text{int}}(k) \propto k^{-3/2}$  and  $E^{\text{kin}}(k) \propto k^{4/3}$  in a wavenumber range  $k_f \sim k \sim \xi^{-1}$  of RUN512. For a closer inspection of the scaling exponent of  $E^{\text{int}}(k)$ , the compensated spectrum  $k^{3/2}E^{\text{int}}(k)$  is plotted in Fig. 3. The slope  $k^{-1/6}$  which corresponds to  $E^{\text{int}}(k) \propto k^{-5/3}$  is given for reference in the figure. The figure shows that the slope of  $E^{\text{int}}(k)$  is closer to  $k^{-3/2}$  rather than  $k^{-5/3}$ .

The scaling  $E^{\text{int}}(k) \propto k^{-3/2}$  is consistent with the weak turbulence analysis by Dyachenko *et al.*<sup>11</sup>. The basic assumptions in the weak turbulence analysis are that the fluctuation of  $\psi$  from its mean is small, *i.e.* Eq. (3),

### Energy Spectra in Quantum Fluid Turbulence

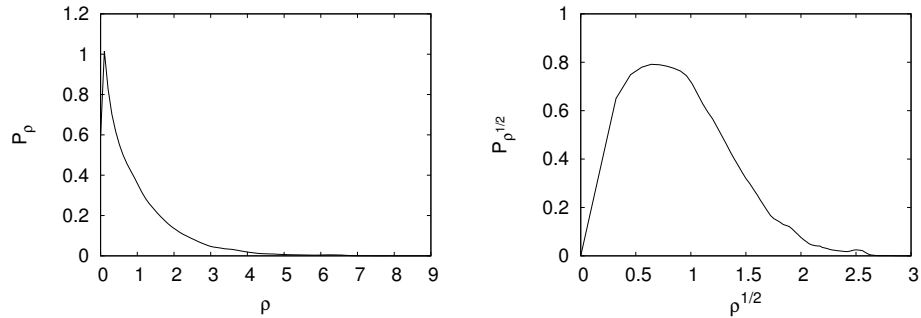


Fig. 4. Probability density function of  $\rho =$  (left) and  $\rho^{1/2} = |\psi|$  (right) in RUN512 at  $t = 24$ .

and that  $\psi$  is approximated by an linear combination of waves with the dispersion relation (4).

### 3.3. Density field

The assumption of the weak turbulence analysis  $|\delta\psi| \ll |\psi_0|$  implies  $|\delta\rho| \ll \bar{\rho}$ . Let us examine the density field  $\rho$  in order to check whether the assumption is valid.

Probability density functions of  $\rho$  and  $\sqrt{\rho} = |\psi|$  are given in Fig. 4 where the samples are taken over grid points in the real space. The figure shows that  $\bar{\rho} (= 1)$  and  $\delta\rho$  are typically of the same order of magnitude. In fact,  $\sqrt{(\overline{\delta\rho})^2} = 1.05$ . The fluctuation  $\delta\rho$  seems to be not small enough for the weak turbulence analysis to be justified.

Figure 5 shows the low density region  $\rho < 0.0025$  in the real space of RUN512 at  $t = 24$ . Note that  $|\delta\rho| \ll \bar{\rho}$  is violated in the low density region. Some parts of the low density region have filament-like structure. It is expected that there are quantized vortex lines inside the structure. The filament-like structure resembles the structure of intense vorticity region observed in direct numerical simulations of classical fluid turbulence. (See, for example, Ref. 12.)

### 3.4. Frequency Spectrum

The validity of the weak turbulence assumption may be tested more directly, in comparison to the density field analysis, by examining the fre-

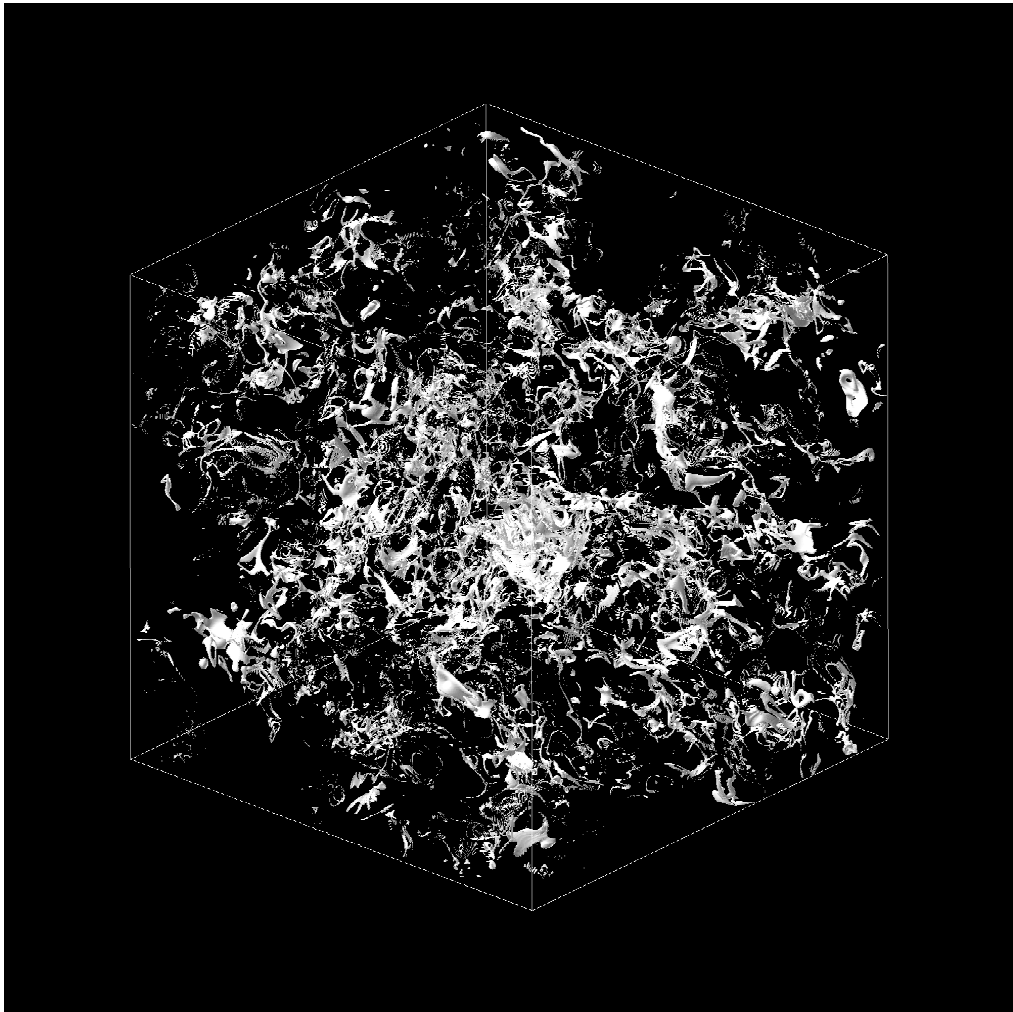


Fig. 5. Low density region  $\rho < 0.0025$  in RUN512 at  $t = 24$ . The whole  $(2\pi)^3$ -domain is displayed.

## Energy Spectra in Quantum Fluid Turbulence

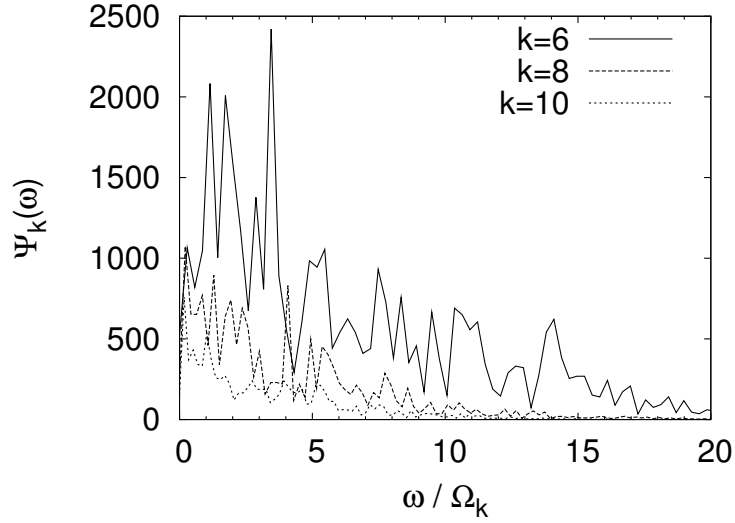


Fig. 6. Averaged frequency spectrum  $\Psi_k(\omega)$  in RUN256.

quency spectrum  $\Psi_{\mathbf{k}}(\omega)$  introduced by

$$\Psi_{\mathbf{k}}(\omega) := \begin{cases} |\psi_{\mathbf{k},\omega}|^2 + |\psi_{\mathbf{k},-\omega}|^2 & (\omega \neq 0) \\ |\psi_{\mathbf{k},\omega}|^2 & (\omega = 0) \end{cases}, \quad (17)$$

where  $\omega = \{0, \Delta\omega, 2\Delta\omega, \dots, (M/2)\Delta\omega\}$ ,  $\Delta\omega := 2\pi/T$ ,  $T$  is a time interval,  $\Delta T$  is a time increment of the time sequence data,  $M := T/\Delta T$ , and  $\psi_{\mathbf{k},\omega}$  is the Fourier transform of  $\psi_{\mathbf{k}}(t)$  with respect to  $t$ , *i.e.*,

$$\psi_{\mathbf{k},\omega} := \frac{1}{2\pi} \int_{t_0}^{t_0+T} dt \psi_{\mathbf{k}}(t) e^{-i\omega(t-t_0)}. \quad (18)$$

In the weak turbulence analysis,  $\psi_{\mathbf{k}}$  is approximated by a wave, *i.e.*,  $\psi_{\mathbf{k}} \sim e^{i(\mathbf{k}\cdot\mathbf{x} + \Omega_{\mathbf{k}}t)}$  with (4). Such an approximation may be appropriate when  $|\bar{\omega}_{\mathbf{k}} - \Omega_{\mathbf{k}}| \ll |\Omega_{\mathbf{k}}|$  and  $\Delta\omega_{\mathbf{k}} \ll |\Omega_{\mathbf{k}}|$ , where

$$\bar{\omega}_{\mathbf{k}} := C_{\mathbf{k}}^{-1} \sum_{\omega} \Delta\omega \omega \Psi_{\mathbf{k}}(\omega), \quad (19)$$

$$\Delta\omega_{\mathbf{k}} := \sqrt{C_{\mathbf{k}}^{-1} \sum_{\omega} \Delta\omega (\omega - \bar{\omega}_{\mathbf{k}})^2 \Psi_{\mathbf{k}}(\omega)}, \quad (20)$$

$$C_{\mathbf{k}} := \sum_{\omega} \Delta\omega \Psi_{\mathbf{k}}(\omega). \quad (21)$$

Figure 6 shows averaged frequency spectra  $\Psi_k(\omega)$  for some wavenumbers  $k$  in the scaling range  $E^{\text{int}}(k) \propto k^{-3/2}$  of RUN256 (See Fig. 2). We used data

from a lower resolution simulation, RUN256, since a long time period data of RUN512 was not available. We put  $T = 102.4$ ,  $\Delta T = 0.1$ ,  $t_0 = 20$  and the average is taken over 4 wavevectors,  $(0, k, 0)$ ,  $(0, -k, 0)$ ,  $(0, 0, k)$ ,  $(0, 0, -k)$ . It is found that the spectrum  $\Psi_{\mathbf{k}}(\omega)$  is not localized around  $|\Omega_k|$ . Typically,  $\bar{\omega}_{\mathbf{k}} \sim \Delta\omega_{\mathbf{k}} \sim 4\Omega_k$ . We may conclude that the present case is outside the scope of the weak turbulence analysis.

#### 4. DISCUSSION

Although the scaling  $E^{\text{int}}(k) \propto k^{-3/2}$  which is consistent with the weak turbulence analysis is observed in the present numerical simulation of GP equation, it turned out from the analysis of the density field and the frequency spectrum that the basic assumptions of the weak turbulence analysis is not satisfied. Therefore, it is difficult to justify the application of the weak turbulence analysis to the present case.

Then, a question arises how the scaling  $E^{\text{int}}(k) \propto k^{-3/2}$  can be explained. Note that the introduction of a wavenumber-dependent time scale  $\tau(k) = \Omega_k^{-1} \sim (\xi k)^{-1}$  is crucial to the derivation of  $E^{\text{int}}(k) \propto k^{-3/2}$  in the weak turbulence analysis. An alternate possible scenario is that the nonlinear effect is not so small as assumed in the weak turbulence analysis and that the wavenumber-dependent time scale  $\tau(k) \sim (\xi k)^{-1}$  is introduced as the correlation time scale, *i.e.*, the time scale of decorrelation due to the nonlinear effect, not as the time scale of the oscillation of the waves.

For classical fluid turbulence, the correlation time scale may be introduced by closure approximations such as the direct interaction approximation (DIA)<sup>13</sup>, the abridged Lagrangian history direct interaction approximation (ALHDIA)<sup>14</sup>, or the Lagrangian renormalized approximation (LRA)<sup>15,16</sup>. DIA deals with the Eulerian correlation time scale, while ALHDIA and LRA deal with the Lagrangian correlation time scale. ALHDIA and LRA derive the Kolmogorov spectrum  $E(k) = C_K \epsilon^{2/3} k^{-5/3}$  up to the Kolmogorov constant  $C_K$  with  $\epsilon$  being the energy dissipation rate, while DIA fails to do so. This implies that one has to choose an appropriate time scale in order to derive the correct energy spectrum. It would be interesting to apply methods similar to DIA, ALHDIA, or LRA to the GP equation and to examine the scalings of the correlation time scale and the energy spectra. This is left for future study.

It is difficult to compare the results of the present GP turbulence simulation directly with those of the experiments of superfluid turbulence (e.g., Refs. 5,6), since (i) the scaling of  $E^{\text{wi}}(k)$  is not observed in the present simulation, and (ii) to our knowledge,  $E^{\text{int}}(k)$  or related quantities are not mea-

## Energy Spectra in Quantum Fluid Turbulence

sured experimentally in superfluid turbulence. The reason for (i) is probably that the forcing in the present simulation injects little to  $E^{\text{wi}}$  of the system, as was discussed in Sec. 3.2.. With regards to  $E^{\text{wi}}$ , the forcing used in the simulation in KT, yielding the Kolmogorov spectrum for  $E^{\text{wi}}(k)$ , might be more relevant to the experiments than the present simulation. As for  $E^{\text{int}}$ , we cannot conclude how much the present simulation is relevant to the experiments at present. It would be interesting to measure  $E^{\text{int}}(k)$  experimentally in superfluid turbulence and to compare it with the present result.

## ACKNOWLEDGMENTS

K.Y. is grateful to S. Nazarenko, M. Kobayashi, and M. Tsubota for stimulating discussion during the workshop on ‘Universal features in turbulence: from quantum to cosmological scales’ in Warwick Turbulence Symposium. The DNSs were performed on a Fujitsu HPC2500 system at the Information Technology Center, Nagoya University. This research is partially supported by Grant-in-Aid for Young Scientists (B) 17740246 from Ministry of Education, Culture, Sports, Science, and Technology of Japan, and by Grant-in-Aid for Scientific Research (B) 17340117 from the Japan Society for the Promotion of Science.

## REFERENCES

1. L.P. Pitaevskii, *Soviet Phys. JETP* **13**, 451 (1961).
2. E.P. Gross, *J. Math. Phys.* **4**, 195 (1963).
3. K.R. Sreenivasan, *Phys. Fluids* **7**, 2778 (1995).
4. Y. Kaneda, T. Ishihara, M. Yokokawa, K. Itakura, and A. Uno. *Phys. Fluids* **15**, L21 (2003).
5. J. Maurer and P. Tabeling, *Europhys. Lett.* **43**, 29 (1998).
6. S.R. Stalp, L. Skrbek, and R.J. Donnelly. *Phys. Rev. Lett.* **82**, 4831 (1999).
7. C. Nore, M. Abid, and M.E. Brachet, *Phys. Fluids* **9**, 2644 (1997).
8. M. Kobayashi and M. Tsubota, *J. Phys. Soc. Jpn.* **74**, 3248 (2005).
9. M. Kobayashi and M. Tsubota, *J. Low Temp. Phys.* this issue.
10. C. Nore, M. Abid, and M.E. Brachet, *Phys. Rev. Lett.*, **78**, 3896(1997).
11. S. Dyachenko, A.C. Newell, A. Pushkarev, and V.E. Zakharov, *Physica D* **57**, 96 (1992).
12. Y. Kaneda and T. Ishihara, *J. Turbulence* **7**(20), 1 (2006).
13. R.H. Kraichnan, *J. Fluid Mech.* **5**, 497 (1959).
14. R.H. Kraichnan, *Phys. Fluids* **8**, 575 (1965).
15. Y. Kaneda, *J. Fluid Mech.* **107**, 131 (1981).
16. Y. Kaneda, *Phys. Fluids* **29**, 701 (1986).